Geophysical Research Letters

Supporting Information for

Advancing Local Distance Discrimination of Explosions and Earthquakes with Joint P/S and M_L-M_C Classification

Ruijia Wang[1,2], Brandon Schmandt[1], Monique Holt[3,4], and Keith Koper[3]

1.Department of Earth & Planetary Sciences, University of New Mexico, Albuquerque, NM, US

2.Department of Earth and Space Sciences, Southern University of Science and Technology, Shenzhen, Guangdong, China

3.Department of Geology and Geophysics, University of Utah, Salt Lake City, Utah, US

4.Department of Earth and Environmental Sciences, University of Illinois at Chicago, Chicago, Illinois, US

Contents of this file

Text S1 to S4
Figures S1 to S9
Table S1

Additional Supporting Information (Files uploaded separately)

Caption for Table S2

Introduction

The supporting information provides details for the local velocity models (Text S1 and Figure S1), datasets (Figure S2–S3, Figure S8–9, also see Table S2 uploaded separately), and processing parameters (Text S2–S3 and Figures S3–S6). The P/S ratio results for SSIP using 3-sec windows are discussed in Text S3 and shown in Figure S4. The optimal P/S ratio and M_L-M_C cutoffs of four datasets are determined based on Area Under the Curve (AUC) from Receiver Operating Characteristic curves (ROC, Figure S5). Figure S6 shows the determination of the best "combined" line by searching over intercept and slopes in the P/S vs. M_L-M_C domain, where best line(s) are chosen based on the maximum AUC. Figure S7 illustrates how the separation of the two populations decreases with station coverage. Figure S8 shows an example of the joint discrimination of the merged dataset with limited station distances (<100 km). Figure S9 includes events that failed quality control (e.g., insufficient M_L or M_C measurements).

Text S1. 1-D Velocity models for the four regions

The 1-D velocity model for MSH is adopted from Kiser *et al.* (2016), where the P and S phases were manually picked from ~3,000 geophones during the controlled source survey (the geophone records are not used in this study). For BASE, we averaged and smoothed the 3D velocity model from Worthington *et al*. (2016) to create the 1-D velocity model for phase prediction. The 1-D velocity model for SPE is adopted from Anderson & Myers (2010). The starting 1-D velocity model of the regional imaging project (Han *et al.*, 2016) is used for SSIP. We merge the crustal models with ak135 (Kennett *et al.*, 1995) at deeper depths (i.e., below the Moho). Lastly, we use the empirical equation from Brocher (2005) to calculate S-wave velocity or density when they are not provided in the original models (Figure S1).

Text S2. Parameter details for P/S ratio calculations and differences to previous studies

Several parameters of P/S calculation and performance evaluation may contribute to our discrimination results:

The P and S phase arrivals are calculated using the corresponding velocity models. The phase windows are scaled with the predicted arrival time differences ($dt = tp - ts$) with two constraints: 1) where $5\%dt$ before and $50\%dt$ after the phases are used; 2) total window lengths between 1–3 sec. In other words, we removed records with phase windows less than 1 sec to avoid potential contamination from phase picking uncertainties. Records at larger distances (~>50km) have a uniform length of 3 sec. The $5\%dt$ buffer window (up to 0.3 sec) before the arrivals is included to mitigate the effects of potential late phase predictions.

As most of the broadband stations have a sampling rate of 40 Hz, we adopted the relatively high and wide frequency band (10–18 Hz) for local distances from Wang *et al*. (2020). Considering our window choices, all phase energy calculations contain at least 10 periods at 10–18 Hz. We refer readers to Wang *et al.* (2020) for more comprehensive and detailed analysis on parameter optimizations (e.g., component, phase window sizes, and frequency band).

In addition to windowing & frequency choices, our method of P/S calculation is different from previous regional studies (e.g., O'Rourke *et al.*, 2016) in a few aspects: 1) all three components are used to calculate phase energy, including transverse for P-waves; 2) no pre-S noise window or S-wave SNR is used; and 3) no MDAC corrections were applied. Such modifications accommodate high-scattering, potential P-coda contamination (to S waves), as well as unsuitable larger-scale corrections at near-distances.

Lastly, our performance evaluation is event-oriented, where TPR and FPR are used instead of variances (e.g., standard deviation from L2 norm; or median absolute deviation from L1 norm). The TPR and FPR (and AUC; or recall and precision) parameters are more resistant to outliers, analogous to event-based L1-norm evaluations. In contrast and for a comparison, the covariance ellipses of the two populations overlap at two standard deviations in the P/S vs. M_L-M_C domain (Figure S7 and S8, also see Figure 4 I the main text). For record-based P/S ratios, the distributions for earthquakes and explosions overlap across most distances like previous studies, even when median absolute deviation is used (Figure S3).

Text S3. P/S ratios for SSIP calculated with 3-sec windows

Considering the significant variation of both topography and Moho depths (Han *et al.*, 2016) in southern California, a slightly wider window (4 sec instead of 3 sec) is used during P/S ratio analysis to account for potential inaccuracies of phase prediction from 1-D velocity model. The 3-sec windows lead to slightly worse discrimination (Figure S4) than 4-sec ones (Figure S3d). We obtained TPR=95.13% and FPR=5.71% with maximum AUC=0.9470 at a P/S cutoff of 0.9. For comparison, when 4-sec phase windows are used, we achieved TPR=97.56% and FPR=0.00% with maximum AUC=0.9818. The number of records also increased (2431 vs. 2754) using 4-sec, suggesting more records reach SNR>2 and a better capture of P

energies in the predicted phase windows. Therefore, the modified window (4-sec) is used for our analysis throughout the main text for SSIP. Other datasets are evaluated with 3-sec windows.

Text S4. Mahalanobis distances (Δ^2) from Multivariate Quadratic Discriminant Function (QDF)

This section introduce the revised Mahalanobis distance calculated from the multivariate quadratic discriminant function (QDF).
For a given sampled event (earthquake or borehole shot), the measured discrimination vector $\boldsymbol{r}$ contains two elements:

$$\boldsymbol{r} = (d_1, d_2)^T, \tag{1}$$

Where, $d_1 = log10(P/S)$, is the array-median P/S ratio and $d_2 = M_L - Mc$ is the array-median magnitude difference. Following Tibi *et al.* (2018) and Tibi (2021), we use the P/S ratio in log scale to ensure they are roughly at comparable range with M_L-M_C. The bivariate Quadratic Discriminant Function (QDF) is then calculated by

$$D(\boldsymbol{r}) = \boldsymbol{r}^T \boldsymbol{A}\boldsymbol{r} + \boldsymbol{B}\boldsymbol{r} + k, \tag{2}$$

in which

$$\boldsymbol{A} = -\frac{1}{2}(\boldsymbol{S_{ex}^{-1}} - \boldsymbol{S_{eq}^{-1}})^T, \tag{3}$$

$$\boldsymbol{B} = \boldsymbol{\mu_{ex}^T S_{ex}^{-1}} - \boldsymbol{\mu_{eq}^T S_{eq}^{-1}}, \tag{4}$$

$$k = -\frac{1}{2}\left[\ln\left(\frac{|\boldsymbol{S_{ex}}|}{|\boldsymbol{S_{eq}}|}\right) + \left(\boldsymbol{\mu_{ex}^T S_{ex}^{-1} \mu_{ex}} - \boldsymbol{\mu_{eq}^T S_{eq}^{-1} \mu_{eq}}\right)\right], \tag{5}$$

Where, $\boldsymbol{\mu_{ex}}$is the mean of $\boldsymbol{R_{ex}} = [\boldsymbol{r_1}\ \boldsymbol{r_2}\ \boldsymbol{r_3}\ \ldots \boldsymbol{r_n}]$ that contains all discrimination vectors for n explosive events; and $\boldsymbol{S_{ex}}$ is the 2×2 ratio covariance matrix for $\boldsymbol{R_{ex}}$. The vectors and matrices with "$\boldsymbol{eq}$" subscripts are defined correspondingly. For a given event, the discrimination score (D) is expected to be positive for explosive sources and negative for earthquakes. The Mahalanobis distance between the two types of events is defined as:

$$\Delta^2 = D(\boldsymbol{\mu_{ex}}) - D\left(\boldsymbol{\mu_{eq}}\right) \tag{6}$$

Taking covariances into consideration, Mahalanobis distance (Δ^2) is a quantitative measure of the "closeness" between two populations in the joint domain (e.g., Figure S6). Lastly, the minimum probability of misclassification P_M, is then calculated using the Mahalanobis distance:

$$P_M = \frac{1}{\sqrt{2\pi}} \int_{-\infty}^{-\Delta/2} e^{-x^2/2}\, dx\ , \tag{7}$$

To evaluate the performance of joint method, only events that have both array-median P/S ratio and M_L-M_C are carried over for the joint discrimination. Thus, the total number (n) of explosives and earthquakes are 68 and 262, respectively. Events that failed to meet the criterion (<3 station-based measurements) are shown Figure S9.

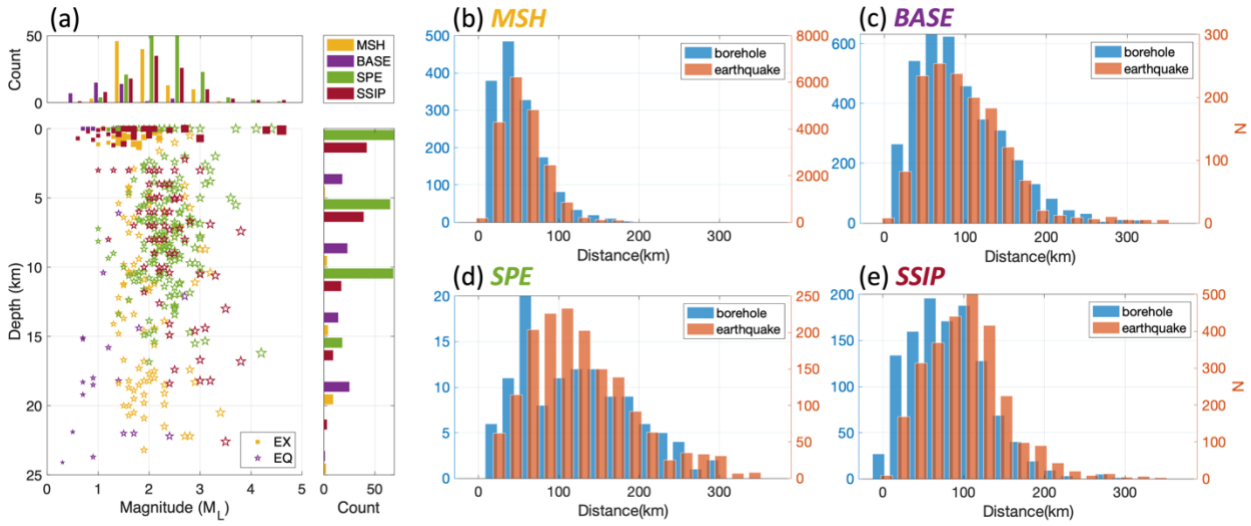

Figure S1. a) Magnitude and event depth distributions for the four datasets (see Figure 1). b–e) event-station distance distributions. EX-explosives (borehole events), EQ-earthquakes.

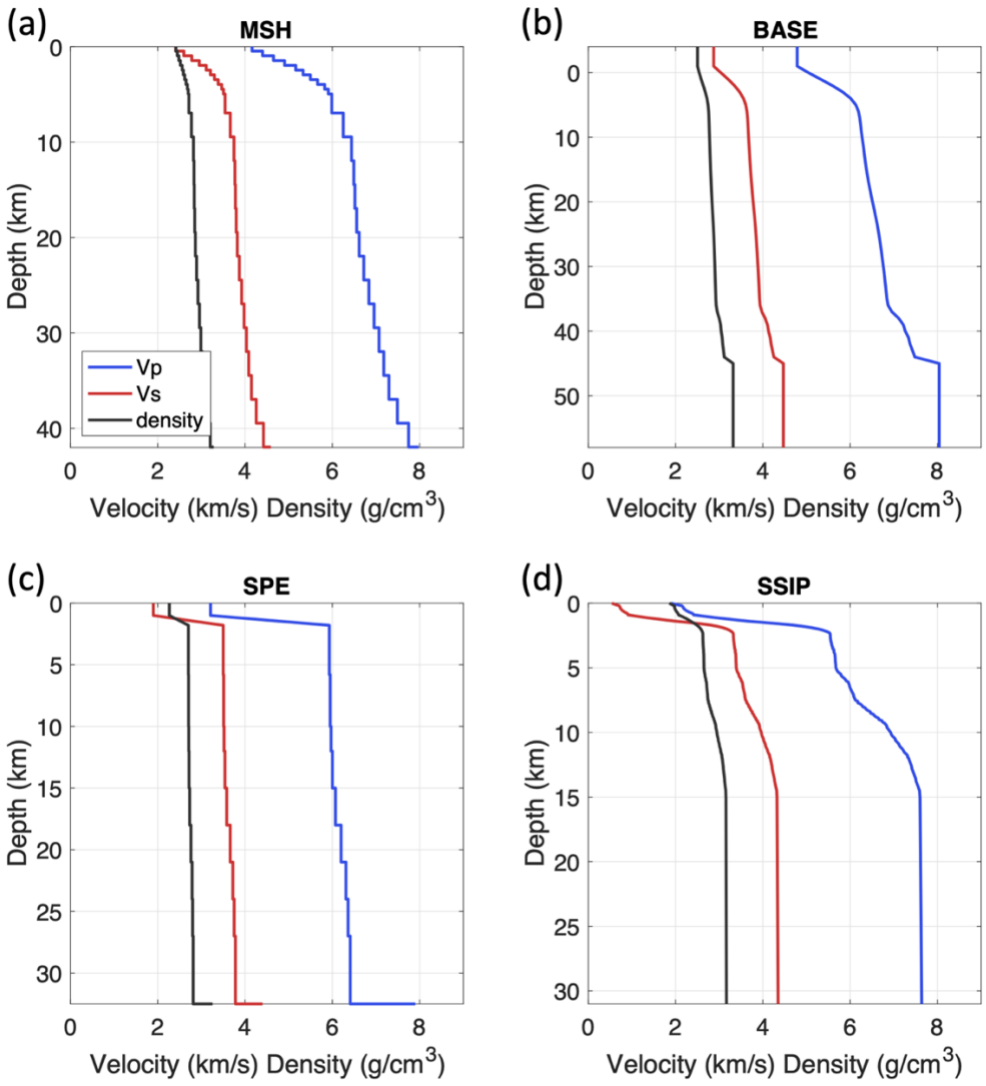

Figure S2. Velocity models used for the four study regions (see Figure 1 in main text).

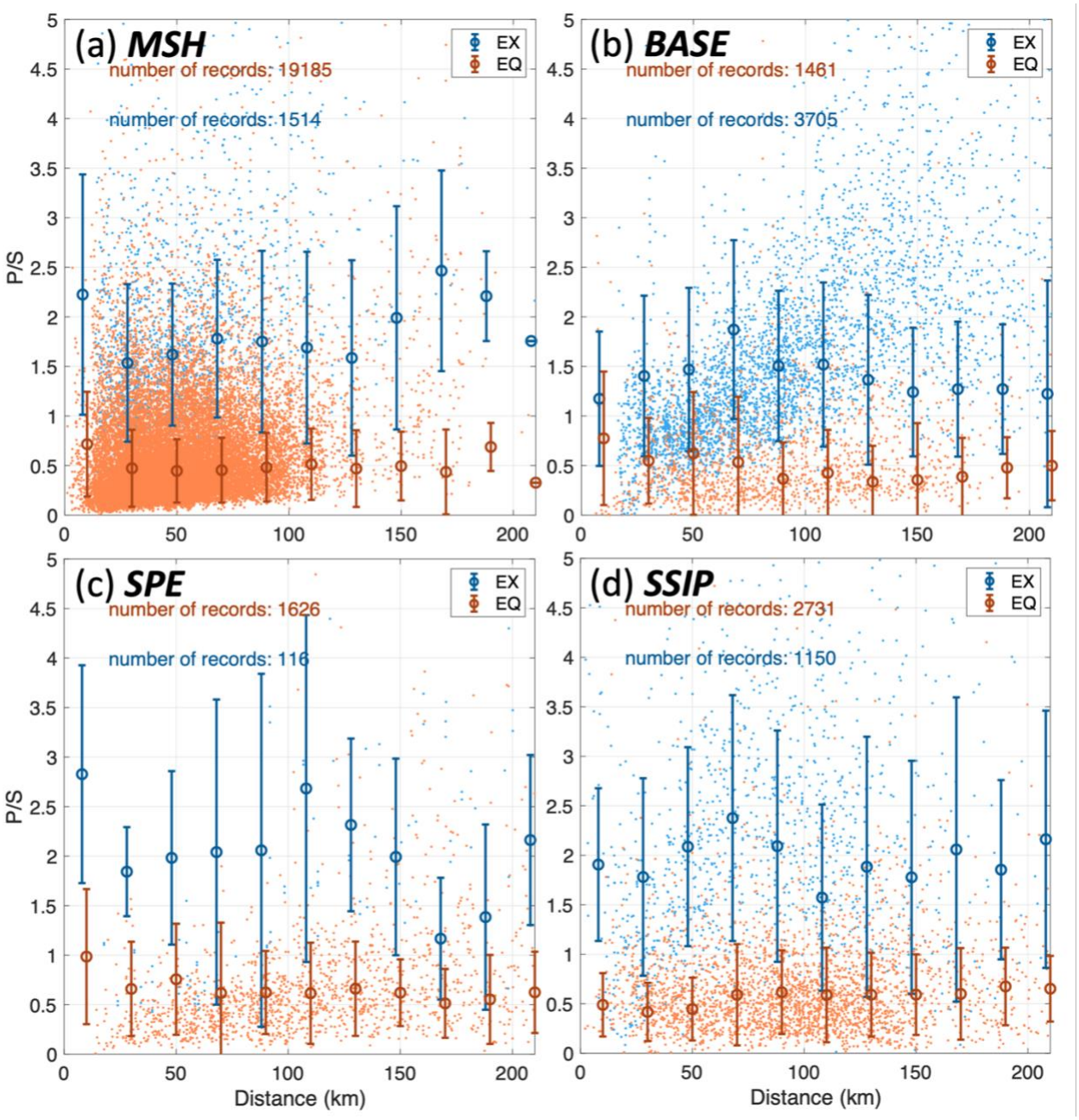

Figure S3. P/S ratio dependence on distances. Distances beyond 200 km are used for calculations but not shown for consistency. The bold bars are average and median absolute deviation for each 20-km bin. EX-explosives (borehole events), EQ-earthquakes.

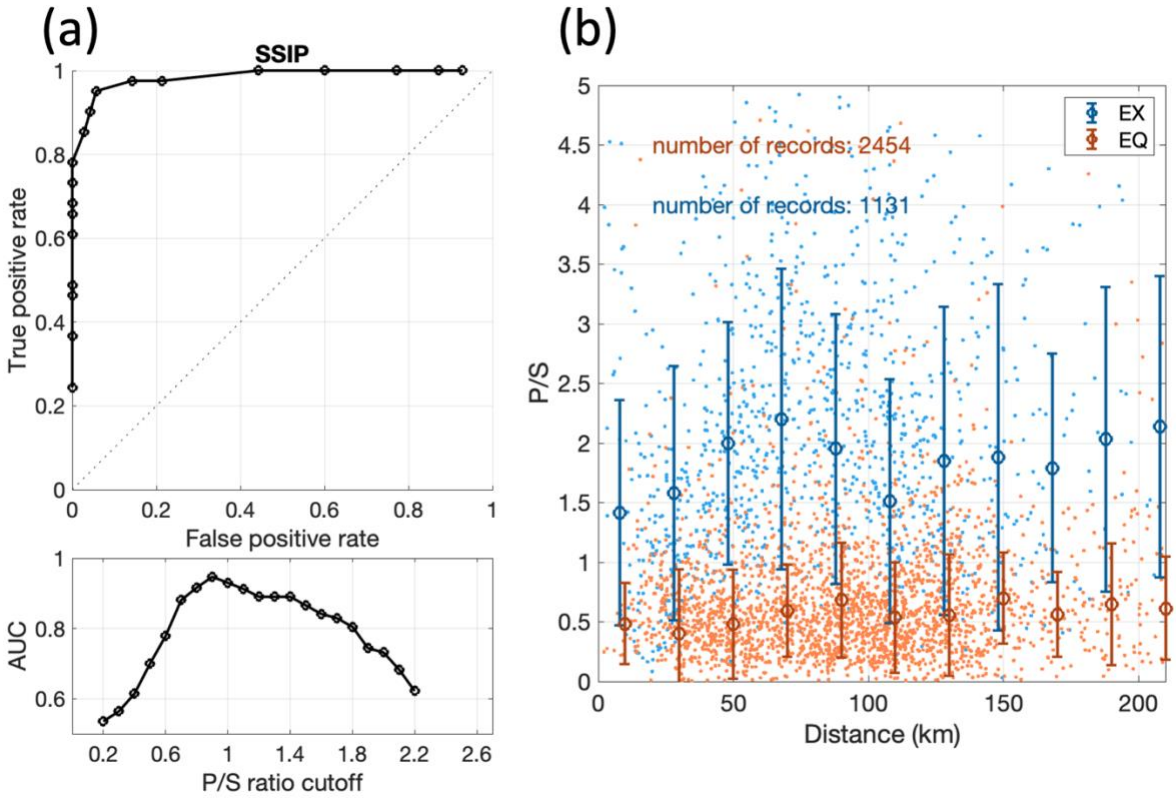

Figure S4. P/S calculation results for SSIP with 3-sec phase windows. a) ROC and AUC curves. Note that the best P/S cutoff peaks at 0.9 instead of 1 (4-sec). b) same as Figure S3d but for 3-sec windows. Note the number of records is lower.

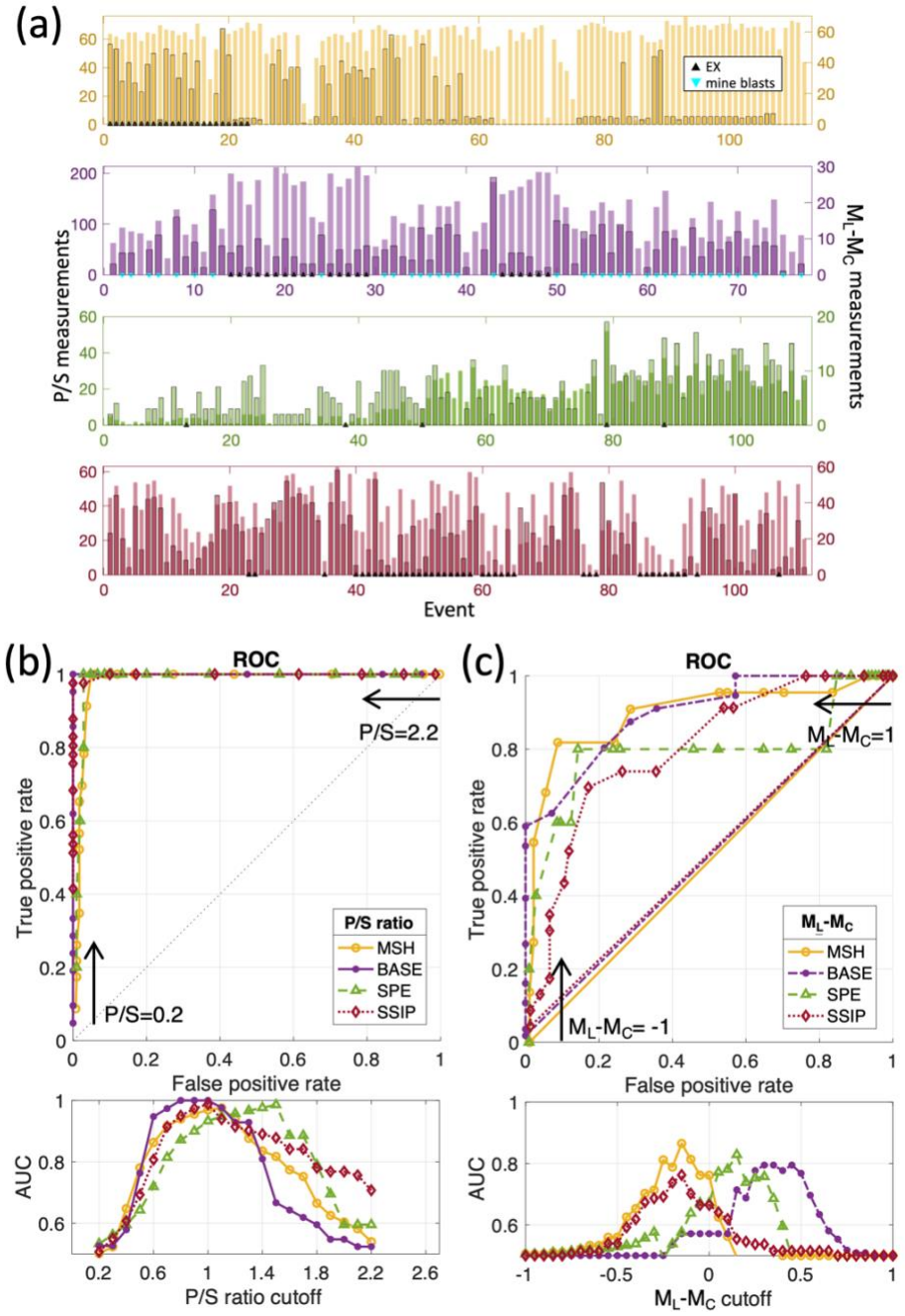

Figure S5. a) Valid number of measurements for both methods (top to bottom, MSH, BASE, SPE, SSIP) . Performance evaluation and best cutoff thresholds for P/S ratio (b) and M_L-M_C (c). Here the TPR and FPR are slightly different from Table 1 in the main text, as events with only valid P/S or M_L-M_C are counted in. In the other word, we do not require an event to have both measurements in this case; Table 1 is showing statistics obtained from the intersection dataset of b) and c). The bottom panels showing AUC as a function of cutoff value are derived by calculating the AUC based on a 3-point curve connecting the lower left corner, the FPR and TPR performance coordinate, and the upper right corner.

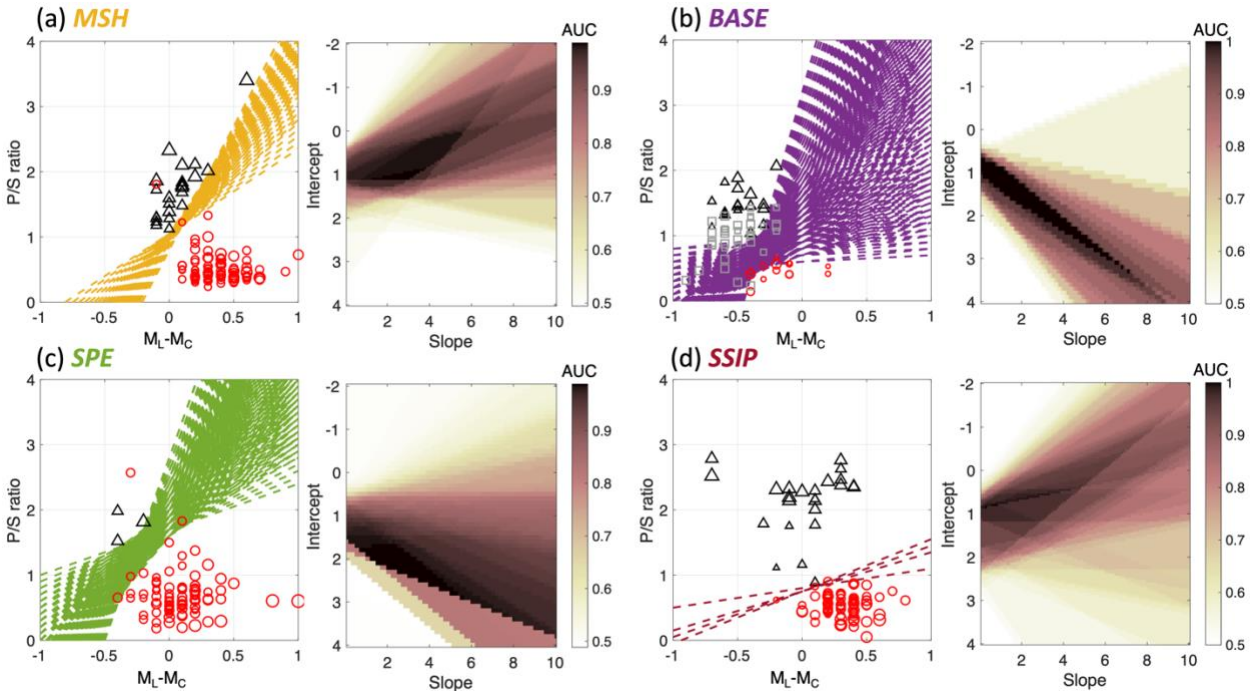

Figure S6. Grid search of slopes and intercepts for the best discrimination "combined" line for the four studied datasets. The color bars are areas under the curve (AUC) from the 2-D ROC analysis. The dashed lines are the combinations of slopes and intercepts that achieve the highest AUCs.

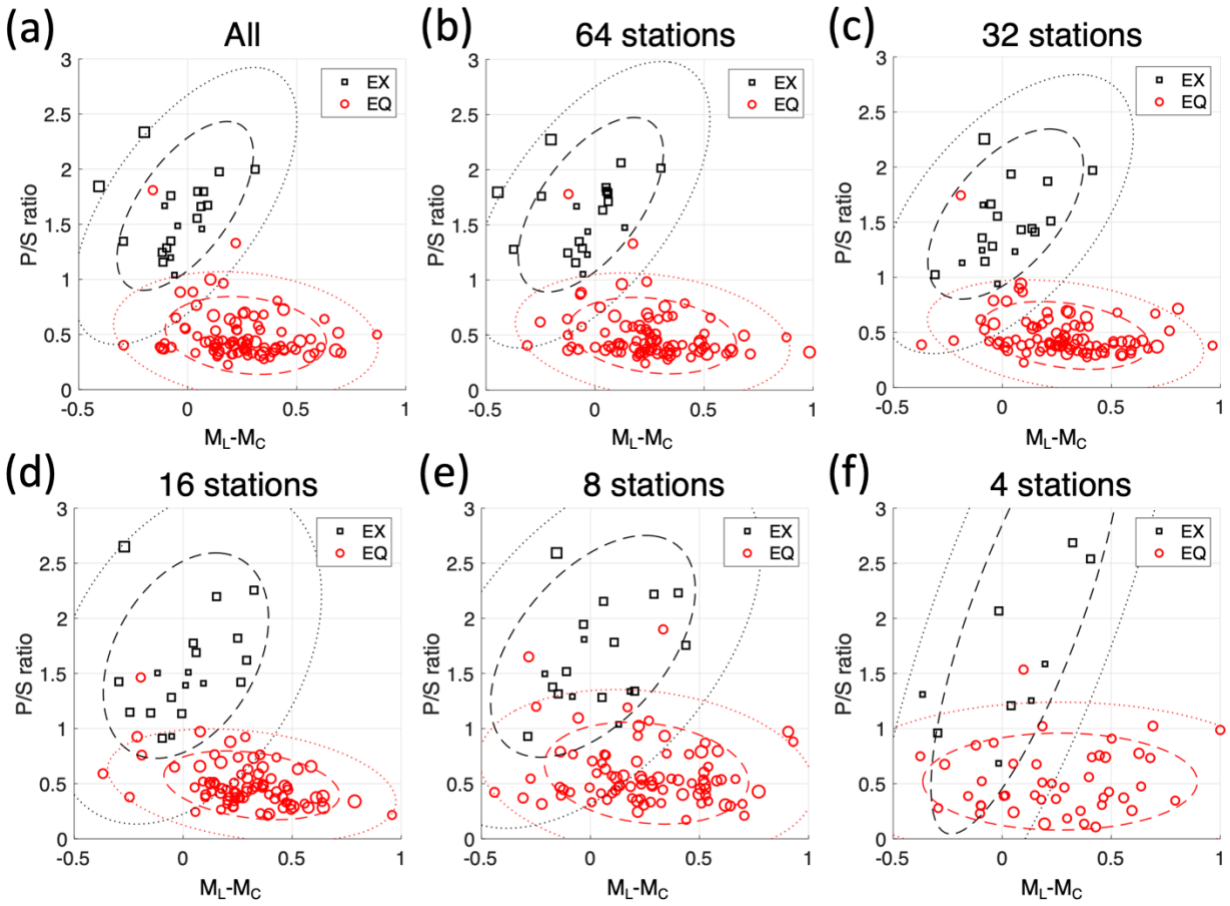

Figure S7. Discrimination performance in the joint domain with decreased stations. The MSH dataset is used for this example (i.e., corresponding to Figure 3a in the main text). In all figures, the dashed and dotted ellipses are the covariance of one and two standard deviations, respectively. Note the overlapped region between the EQ and EX ellipses increases with decreased station number, which will be quantified as lower Mahalanobis distances.

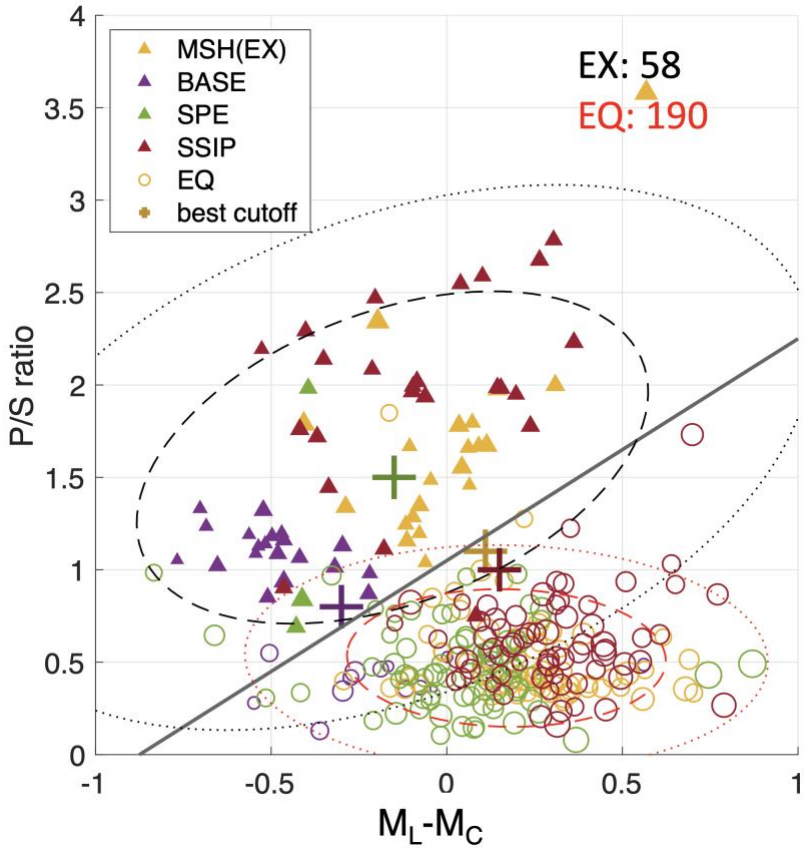

Figure S8. Discrimination results in the joint coordinate using stations within 100 km (i.e., same as Figure 4a in the main text but limiting to 100 km). (a) All event-based P/S or M_L-M_C of the four datasets as labeled. The cross symbols mark the best P/S and M_L-M_C cut offs for each dataset, determined from the ROC and AUC curves (see Figure 2). The dashed and dotted ellipses are the covariance of one and two standard deviations, respectively. The grey line marks the best joint discrimination threshold.

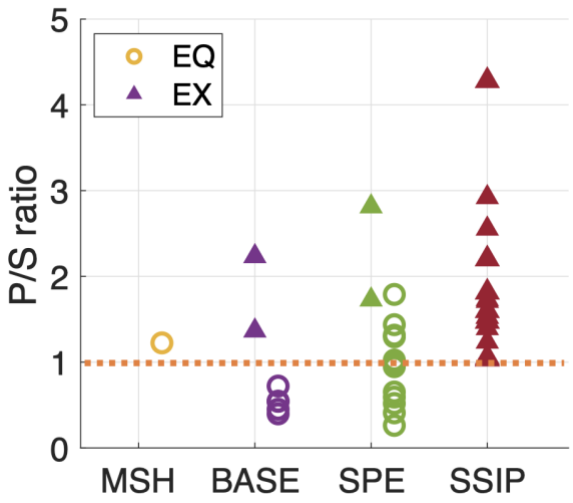

Figure S9. P/S ratio for the 23 earthquakes and 21 explosive events that are not analyzed in the joint domain due to low (<3) or missing valid stations. Five earthquakes from SPE are missing P/S measurements, thus, are not shown. The orange dotted line marks an optimal P/S cutoff of 1.

Table S1. Explosives reported as earthquakes by USGS from SSIP. The reported origin times of the six events are within 0.2–2.4 sec of and co-located with the six shots on March 6, 2011.

Catalog Time (UTC)	**Catalog Latitude**	**Catalog Longitude**	**Catalog Depth**	**Catalog M_L**	***Shot ID***	***True time (UTC)***	***True Latitude***	***True Longitude***	***Load (kg)***
2011-03-06 12:09:02.400	32.703	-115.260	10	2	*10460*	*12:09*	*32.69438*	*-115.25193*	1367
2011-03-06 10:33:00.400	32.677	-116.386	3	1.8	*20550*	*10:33*	*32.67207*	*-116.34656*	*911*
2011-03-06 10:12:01.620	32.841	-115.367	13	1.7	*10670*	*12:12*	*32.84924*	*-115.3718*	458
2011-03-06 10:09:01.370	32.981	-115.205	4.8	1.7	*21640*	*10:09*	*32.9638338*	*-115.2313188*	*592*
2011-03-06 09:02:59.800	32.59	-116.693	0.6	1.5	*20220*	*09:03*	*32.6008*	*-116.68154*	*684*
2011-03-06 07:15:01.490	32.879	-115.535	17.2	2.1	*21330*	*07:15*	*32.8851499*	*-115.5409971*	*911*

Table S2. [uploaded separately] Datasets showing all the events and explosives used for the four regions, with event-based P/S, M_L, and M_C calculated (as well as the number of stations used for each measurement). For the "Source Type" in the last column of each sheet: 0-explosive, 1-earthquake, 4-mine blast.